Confidential: not for distribution. Submitted to Institute of Physics Publishing for peer review on 17 October 2006

A Multi-Scale Model for Mobile and Localized Electroluminescence in Carbon Nanotube Field-Effect Transistors

D L McGuire and D L Pulfrey

UBC Dept. of E&CE, 2332 Main Mall, Vancouver, BC, Canada V6T 1Z4. Phone: +1 604 822 2183. Fax: +1 604 822 5949

E-mail: pulfrey@ece.ubc.ca

Abstract. A multi-scale model is presented that captures the experimentally observed behviour of electroluminescence (EL) in carbon nanotube field-effect transistors (CNFETs) under ambipolar bias conditions, namely variations in mobile EL intensity, localized EL at a contact, and localized EL at a charge defect. A full, quantum mechanical approach is used to describe tunneling and thermionic emission at the contacts, and the drift-diffusion equations, with a field dependent mobility, are used for transport in the long devices (CN length $\geq 10\mu$m). We find that contact-localized EL is only present when the height of the Schottky barrier at the ends of the CN favours the injection of one type of carrier. Charge defects on the CN surface also lead to localized EL, which is present only under certain bias conditions.

Submitted to: *Nanotechnology*

1. Introduction

Electroluminescence (EL) from carbon nanotube field-effect transistors (CNFETs) has recently been demonstrated [1–5]. Initial reports on EL were of a mobile light spot with a width of $\approx 5\mu$m that could be positioned longitudinally along the CN by varying the gate bias [1, 2]. The intensity of this mobile luminescence increased as the spot neared the contacts [2]. Most recently, localized luminescence at a contact and at defect sites has been reported [3]. Both free-carrier recombination and exciton relaxation have been proposed as possible radiation mechanisms. In this paper, we present a multi-scale model in which only free-carrier, band-to-band recombination is considered, but which is able to predict all of the experimentally observed EL phenomena in non-looping CNs.

Light spot mobility in long-channel devices under ambipolar bias conditions has been modeled by Tersoff *et al.* using a simple analytic drift-current expression that assumes a negligible recombination length [6]. That model captures the movement of the emission spot but fails to account for the peaking in intensity of the mobile emission near the contacts. Guo *et al.* solved the drift-diffusion, continuity and Poisson equations self-consistently, but did not investigate many of the observed EL effects [7]. The model presented in this work improves on other models in that it does not assume a negligible recombination length [6]; it uses a full quantum mechanical treatment for carrier injection, rather than a WKB approximation for tunneling and thermionic emission [7]; and it uses a field-dependent mobility, rather than an arbitrary, constant mobility [7]. By using a Schottky-barrier (SB) height for the source and drain contacts that is more appropriate to the palladium contacts used experimentally [2, 3], localized emission at one contact can be predicted. Introduction of a charged defect in the tube, which obviously will affect the electrostatics [8], is also shown to create a site of localized emission, as reported in [3].

2. Model

Although the experimental devices are planar [2, 3], we follow the approach of Guo *et al.* and evaluate co-axial structures [7], due to their relative ease of simulation [9]. The simulation space is shown below in figure 1 and is closed by null-Neumann boundaries. The length of the contacts l_{sd} is chosen to be sufficiently large as to minimize the error introduced by these non-physical boundary conditions [10].

A multi-scale model is required because the transport of interest is both quantum mechanical and classical in nature. At the SB source and drain contacts, quantum mechanical tunneling and reflection occurs, while transport in the long CN channel ($l_{cn} \geq 10\mu$m) is diffusive in nature. Further, the acoustical phonon mean free path is on the order of 300nm, which suggests that approximating the carriers involved in long-range transport as being thermalized is appropriate [11]. Therefore, the model presented in this paper combines solvers for the effective-mass Schrödinger wave equation (SWE) and the drift-diffusion and continuity equations (DDE/CE). The effective-mass is taken

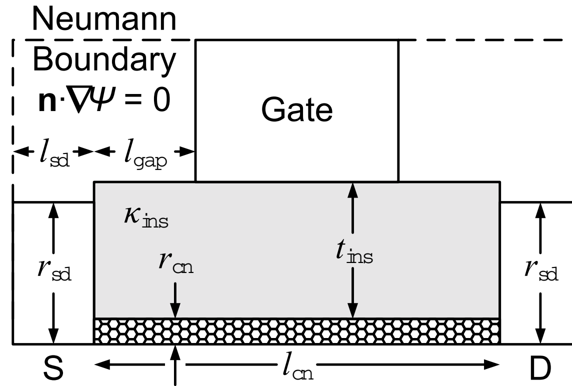

Figure 1. CNFET geometry.

from a fit to the band structure, as obtained from the nearest-neighbour tight-binding approximation [12]. In the region near the contact, where quantum mechanical tunneling and thermionic emission are significant, the solution to the SWE gives a transmission probability. The interface currents are computed from the Landauer equation for the case of a single, doubly-degenerate band (*e.g.* electrons at the source). For the thermionic emission current,

$$I_{\mathrm{TE}} = -\frac{4q}{h}\int_{E_{\mathrm{c}}(0)}^{E_{\max}} T(E)\left(f_{\mu_{\mathrm{S}}}(E) - f_{\phi_{\mathrm{N}}}(E)\right)\,\mathrm{d}E \tag{1}$$

where $T(E)$ is the transmission probability, μ_S refers to the source Fermi level, and ϕ_N is the electron quasi-Fermi level, which is obtained self-consistently from our solver. The SB at the CN-contact interface is treated phenomenologically via the difference between the metal work function and the CN electron affinity [12]. The energy range in this example is taken to extend above the barrier from the conduction band edge at the CN-contact interface $E_{\mathrm{c}}(0)$ to a maximum energy chosen to capture all significant carriers ($E_{\max} = \mu_{\mathrm{S}} + 20kT$).

The tunneling current can be conveniently incorporated into our multi-scale model by representing it as a generation rate, as described in [13] and adapted as follows (the electron case is given as an example here, however only minor modifications are necessary to treat holes): transforming the continuity equation,

$$G_{\mathrm{TUN,n}}(z) = -\frac{1}{q}\nabla\cdot J_{\mathrm{TUN,n}} = \frac{\mathrm{d}J_{\mathrm{TUN,n}}}{\mathrm{d}E}\cdot\nabla\psi\,, \tag{2}$$

the generation rate $G_{\mathrm{TUN,n}}$ can be expressed in terms of the gradient of the tunneling current with respect to energy $E = -q\psi$ and the gradient of the potential on the CN surface $\nabla\psi$. Using the Landauer equation for the tunneling current, we obtain an expression for the generation rate that depends on the transmission probability $T(E)$ obtained from the SWE solution,

$$G_{\mathrm{TUN,n}}(z) = -\frac{4q}{h}\,T\left(E_{\mathrm{c}}(z)\right)\left[f_{\mu_{\mathrm{S}}}\left(E_{\mathrm{c}}(z)\right) - f_{\phi_{\mathrm{N}}}\left(E_{\mathrm{c}}(z)\right)\right]\frac{\mathrm{d}\psi}{\mathrm{d}z}\,, \tag{3}$$

where conduction band energy $E_c(z)$ links energy and position. The situation for the currents at the injecting contact is illustrated in figure 2.

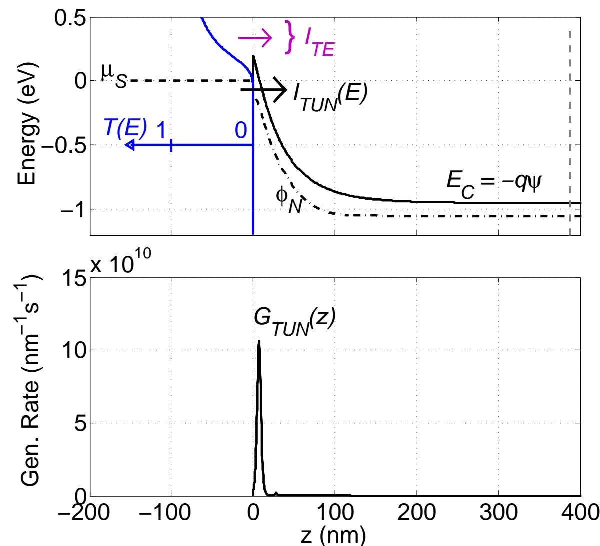

Figure 2. Top graph: Schottky barrier at the contact-CN interface ($z = 0\,\mathrm{nm}$). The large wavevector discontinuity leads to $T(E) < 1$, even above the barrier ($T(E)$ in blue on a rotated axis). The quantum mechanical region is bounded (dashed grey line) at $z \approx 380\mathrm{nm}$; at this point, the electric field is less than a minimum tolerance. Bottom graph: $G_{\mathrm{TUN}}(z)$ as computed from the transmission probability $T(E)$ [13]. At the source, only electrons are generated (as opposed to EHPs).

The electrostatic potential for the CNFET is supplied by the Poisson equation, which takes its charge input from the tunneling generation rates G_{TUN} and the DDE/CE solutions n and p, where the thermionic emission current is used as a Neumann boundary condition. Thus, the the iterative solution involves the SWE, DDE/CE and the Poisson equation, but any injected charge that does not contribute directly to the current, *i.e.*, evanescent solutions to the SWE, is not considered. In addition, the contacts are assumed to be ideal sources/sinks of carriers.

The recombination of electrons and holes is related to the current density on the CN surface by the continuity equations,

$$\frac{1}{q}\nabla \cdot \mathbf{J}_{\mathrm{n}} = R - G_{\mathrm{TUN,n}} \qquad \frac{1}{q}\nabla \cdot \mathbf{J}_{\mathrm{p}} = -R + G_{\mathrm{TUN,p}}\,, \tag{4}$$

where the generation terms G_{TUN} represent the electron (n) and hole (p) tunneling currents, as described above, and R is the net recombination rate, given by the sum of band-to-band, radiative recombination and band-to-band generation, such that

$$R = B(np - n_i^2)\,. \tag{5}$$

The current density $\mathbf{J}$, recombination rate R, generation rates G_{TUN}, and carrier concentrations n and p are each position-dependent. In 5, B is the direct radiative recombination velocity. As described in the Results section, we ascribe a constant value

to B based on a fit to experimental data. We do not attempt to explicitly model other recombination mechanisms, such as Auger [14] or exciton relaxation [4,15], that may be operative.

Charge transport is restricted to the CN surface, such that the DDEs and CEs are solved in one dimension. Transport is assumed to be unidirectional in the case of each carrier (*i.e.*, source-injected electrons and drain-injected holes). At the collecting contact, an infinite recombination velocity is assumed. This implies that a Dirichlet boundary is set by the intrinsic carrier concentration n_{i}, for which we ascribe a value using an effective-mass density of states [12].

As there is a significant variation in the electric field along the length of the CN, it is important to include that dependence in the electron and hole mobilities $\mu(\mathbf{E})$. Under low-field conditions, CNs are expected to demonstrate near-ballistic behaviour [16]. Under the influence of larger fields, carrier behaviour is less well understood. Theoretical predictions suggest negative differential mobility may arise from electron transfer between subbands [17,18], and that optical phonons, whose mean-free-path is in the range of 10-100 nm, may be excited [19]. Experimentally, mobilities have been reported between $10\,\mathrm{cm}^2/\mathrm{V}$-s and $100,000\,\mathrm{cm}^2/\mathrm{V}$-s [16,20]. An analysis based on electrons scattering by longitudinal acoustic (LA) phonons found low-field mobilities in reasonable agreement with the experimental results [17]. This theoretical result is used to describe the mobility of the electrons and holes in the CN channel in this paper. Under the bias conditions used in our simulations, the electric field strength ranges from 0.01-100 kV/cm and mobilities vary from $20,000$-$20\,\mathrm{cm}^2/\mathrm{V}$-s.

3. Simulation Method

A damped iterative method is used to seek a convergent numerical solution to the system of equations given in the previous section. The equations are approximated by the finite difference method on a variably-spaced mesh. The Laplace solution is used to initialize the simulation along with an estimate of carrier concentration distributions from a previously converged simulation when available (otherwise, intrinsic carrier concentrations are used). Due to the exponential nature of the equations and their interdepdenence, convergence is difficult to obtain, and large oscillations in charge tend to destabilize the simulation. To overcome this difficulty, memory was incorporated into the charge estimates n_k and p_k such that

$$n_k = wn_{k-1} + (1-w)n_{k-2} \tag{6}$$

$$p_k = wp_{k-1} + (1-w)p_{k-2}\,, \tag{7}$$

where w is a weighting factor (typically, $w = 0.5$) and k is the iteration index. This technique dramatically improves convergence over a wide range of cases without significantly impacting the simulation time. Once the charge residual has reached an intermediate tolerance, *e.g.*, a factor of 10^2 larger than the final tolerance, the weighting can be shifted to favour the nearest charge estimate to improve convergence

rates. Updates to the electrostatic potential are obtained by linearizing the potential and computing the difference based on the latest charge estimate. Convergence is obtained when voltage and charge residuals meet specified abolute tolerances. Charge tolerances must be tight enough such that the location where the net charge is zero, *i.e.* $Q_{\rm net} = p - n = 0$, stabilizes.

4. Results and Discussion

Results are reported that relate to three features of EL observed recently in experimental devices and not described by previous models [6, 7], namely variations in intensity of the mobile luminescence [2], localized light emission at one of the contacts [3], and localized EL at space-charge regions induced by charge defects in the oxide [3]. The dimensions of the device shown in figure 1 are chosen to capture the critical characteristics of the experimental devices in [2, 3]; these parameters are listed in table 1. In the presentation of these results, the photon emission rate is attributed to the recombination rate R obtained from self-consistent simulation: we normalize R to the bandgap energy $E_{\rm g} = 0.4$eV (*i.e.*, the emission spectrum), and assume a photon emission efficiency of 10^{-4} as in an excitonic process [4]. A constant drain current (0.2μA in our simulations) was maintained while $V_{\rm DS}$ and $V_{\rm GS}$ were varied, consistent with the biasing scheme of the experimental work [2]. B was determined by fitting the width of the simulated luminescence peak to the experimental result at the half-power level as shown in figure 3. The source-drain bias voltages employed in these simulations range from $0.5-2.5$V, leading to reduced carrier concentrations in the channel when compared to those expected for the biases used in the experiments [2, 3]. Evidence of this is seen in the lowered drain current: $I_D = 0.2\,\mu$A in simulations compared to $I_D \simeq 18\,\mu$A in experiments [2]. Comparisons of absolute intensities of photon emission are confounded by the reduced-dimension approach of the simulations as well as by variations between experimental designs, however some relative measures may be evaluated, as described below.

4.1. Mobile Electroluminescence

We begin by noting that the recombination term R (see 5) depends on the charge product np. Luminescence intensity measurements reported in the work of Freitag *et al.* indicate a peaking of emission as the light spot approaches the contact [2]. In their work, the authors suggest that this may be from injected carriers at higher energies that scatter and emit photons at energies greater than the bandgap. Simulations using our multi-scale model demonstrate that this peaking, as shown in figure 4, can result solely from the consideration of ambipolar transport. While the shift in the bias (lowering $V_{\rm GS}$ relative to V_{DS}) increases the population of holes relative to the populations of electrons, the low mobility in the high-field region near the contact, coupled with the continued presence of electrons, leads to a peaking in the intensity of the light spot. Freitag *et al.*

Table 1. Device parameters

Device	1	2	3
r_{cn} (nm)	1	1	1
l_{cn} (μm)	50	10	20
t_{ins} (nm)	100	10	100
r_{sd} (nm)	30	15	30
l_{sd} (nm)	10	10	10
l_{gap} (nm)	10	10	10
κ_{ins}	3.9	3.9	3.9
Chirality	(25,0)	(25,0)	(25,0)
E_{g} (eV)	0.4	0.4	0.4
ϕ_{Bp} (eV)	0.2	0.05	0.2

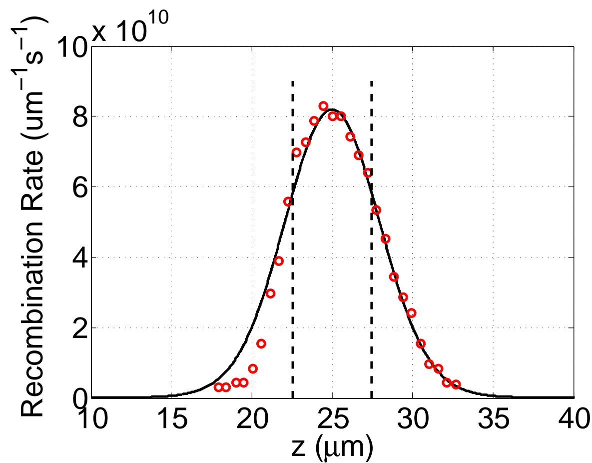

Figure 3. Comparision of the simulated emission peak R (solid) with the measured rate (red circles) of [2]. Measured emission is in arbitrary units and its height is scaled so that both peaks have the same value. B is then determined by matching the width of both peaks at half-power (dashed bars).

report that the intensity of mobile luminescence is approximately 20% higher near the contact than at mid-tube [2]. In our simulations, the intensity increases by 14%. Looking at the recombination profile in figure 4, the peak intensity remains constant once the peak location moves more than $\approx 8\mu$m from the contact. In this middle length of the CN, the electric field is low, and the mobility typically reaches its peak value. This is in contrast to the experiments, which relied on much higher biases, and would therefore expect lower mobilities. It is important to note that the simulated recombination rate R is approximately six orders larger than the experimentally observed result for the actual light intensity [2]. When normalized to the bandgap energy and scaled by emission efficiency, the peak simulated emission rate at the mid-channel bias point compares well

to the experimental result: it is a factor of four smaller than reported in [2].

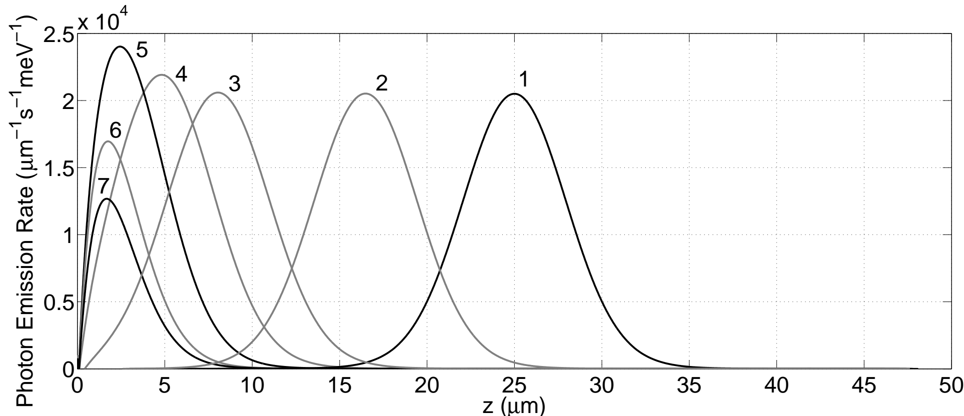

Figure 4. Simulated photon emission rate under varying bias, constant current ($I_{\rm D} = 0.2\mu$A) for device 1 (see table 1). Emission efficiency is assumed to be 10^{-4} [4] and the result is normalized to the bandgap energy $E_g = 0.4$eV. Central bias point (peak #1 at $z = 25\mu$m) $V_{\rm DS} = 2 \times V_{\rm GS} = 2.3$V. Second and third highlighted curves (near $z = 5\mu$m) illustrate emission peaking (peak #5, $V_{\rm DS} = 2.183 \times V_{\rm GS} = 2.286$V) and decay as device operation become more unipolar (peak #7, $V_{\rm DS} = 2.703 \times V_{\rm GS} = 2.141$V).

4.2. Fixed Bright Spot at Contact

To consider the effects of the contacts on the luminescence profiles, we vary the SB height at the contacts to make the device more unipolar in operation (as in device 2, table 1), such that the CNFET operates as a p-type device, with $\phi_{\rm Bp} = 0.05$eV. Our simulations show a localized luminescence with high intensity that develops at the drain contact, as shown in figure 5. Injection of holes at the drain forms a large positive charge that pulls the bands down sharply. This creates an electric field that retards the exit of electrons from the device at the drain. The pile up of both types of carriers enhances recombination, resulting in a strong emission peak. A representative band diagram and charge profile are shown in figure 6. This contact-related phenomenon is very strong, and persists even when more gate control of the electrostatics is introduced by thinning the oxide (device 2, table 1). It is important to note that as the bias is varied, we continue to observe the motion of the mobile light spot in the manner outlined previously. The intensity of the mobile light spot remains similar to that previously reported, while the bright spot at the contact is approximately a factor of six larger in intensity.

Varying results on localized luminescence at a contact have been reported, including the absence of such a persistent bright-spot [2]. We did not observe persistent EL at a contact when representing the SB with a barrier height equal to half the bandgap [7]. Our observance of contact-localized EL with a lower $\phi_{\rm Bp}$ suggests that the phenomenological modeling of the contact as a simple barrier may need improvement. Such SB models have proven adequate at capturing a broad range of electronic effects,

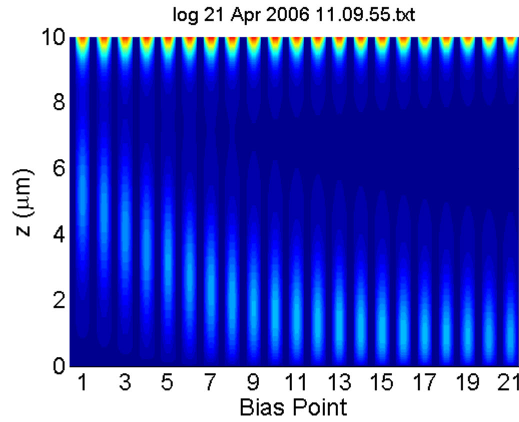

Figure 5. Bright, fixed-location emission peak at the drain contact for a p-type device ($\phi_B = 0.05$eV for holes). Constant current $I_{\mathrm{D}} = 0.2\mu$A, $V_{\mathrm{DS}} = 1.42 \times V_{\mathrm{GS}} = 0.665$V at the bias point 1. Recombination profile shows the varying position of the mobile light spot ($z = 0 - 5\mu$m) as well as the persistent bright emission at the drain ($z = 10\mu$m).

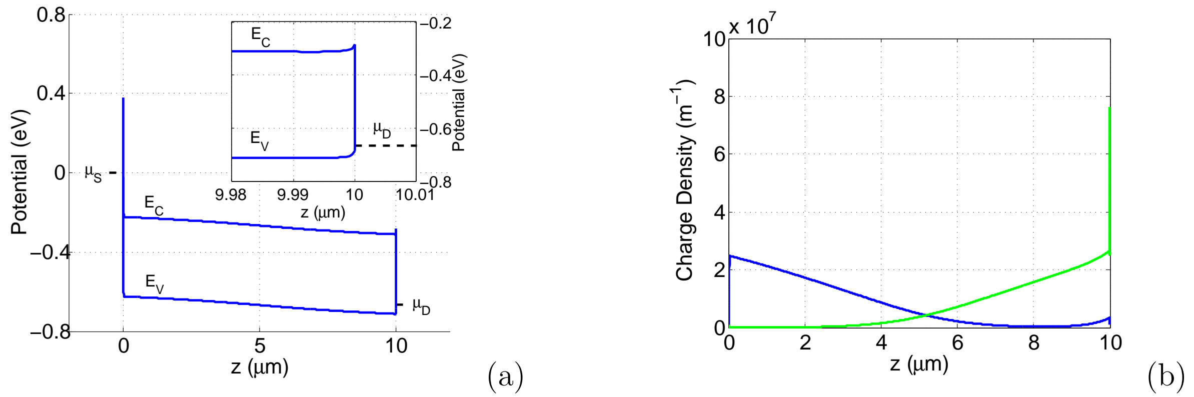

Figure 6. Energy bands (a) and carrier density (b) for bias point 1 (figure 5, $V_{\mathrm{DS}} = 1.42 \times V_{\mathrm{GS}} = 0.665$V). Energy bands (a) show strong band bending at drain, creating a barrier to electrons exiting the CN (see inset, (a)), causing pile-up. The low barrier to holes ($\phi_{\mathrm{Bp}} = 0.05$eV) leads to significant hole injection and a large recombination rate. Corresponding carrier density profile (b) showing electrons (blue, left) and holes (green, right).

and have proved valuable in device modelling when exploring the performance limits of proposed devices [9, 21, 22]. However, the strength of the contact-localized EL observed in this model depends strongly on the SB height, and this may offer a means to better characterize the contact-CN interface.

In comparison with the experimental devices of Freitag *et al.*, we note that both palladium and palladium with a titanium adhesion layer were used as contacts [2, 3]. Titanium contacts would form a small positive barrier to holes, similar to the ϕ_{B} used in these simulations, while palladium on its own would induce a negative barrier to holes, enchancing the observed effect [23]. Previous experimental work suggested that

the barrier heights to both electrons and holes were significantly reduced when titanium contacts were used due to barrier thinning from strong electric fields [24]. Further simulations at a range of barrier heights indicate that, under the bias conditions used, a fixed bright peak is present for $\phi_{\rm B} \lesssim 0.1$eV. This of course is dependent upon the magnitude of the gate-induced electric field and the separation between the gate and source/drain contacts, which, in turn, influence the thickness of the tunneling barrier.

4.3. Fixed Bright Spot at Defects

A fixed-point defect was simulated by introducing a charge of +0.2e on the surface of the CN at distance of 6μm from the source contact (device 3, table 1). The EL results are shown in figure 7a, from which it is clear that, in addition to the usual mobile EL, fixed EL appears at the defect site once certain bias conditions are met. In our simulations of defect-localized EL, the Zener effect is not considered as a possible means for electron excitation, neither is impact excitation of excitons from the strong field, as was proposeded in [3]. Here, the p-type defect creates an electron trap (figure 7c), therefore we would expect that a hole-dominant bias would be required to induce defect-localized EL. As clearly shown in figure 7b, a majority population of holes is required at the defect to observe localized EL. This confirms the requirement of polarity from [3], however, in our model, the EL is solely a by-product of radiative free-carrier band-to-band recombination in a diffusive system.

On the surface of the CN, the charge defect causes band-bending, which acts as a trap for carriers. From the plot of the carrier distribution (figure 7b), we observe a strong peak in the electron density at the defect due to carrier trapping, as expected. With the mobile light spot beginning at the drain end (z = 20μm, figure 7a - bias point 1), electrons are the dominant carrier, and few holes are present in the CN. In this situation, there is no emission at the defect location. As hole injection increases, the mobile light spot moves towards the defect (see bias points 2 to 6, figure 7a), but with no presence of holes near the defect, no stationary, localized EL developes. As the bias is changed to further favour hole injection (green arrow, figure 7d), holes are blocked by the electric field barrier that results from defect-induced band-bending. This forms a region of further positive charge located next to the defect, which then pulls the bands down (black arrow, figure 7d). As the mobile light spot approaches the defect location, electrons trapped at the p-type defect and injected electrons recombine with the growing population of injected holes, leading to the formation of a defect-localized bright spot (see bias points 7 and 8, figure 7a). This localized EL persists as the mobile spot moves past the defect towards the source (see bias points 9-13, figure 7a) due to the strong hole injection and continued presence of electrons at the defect location.

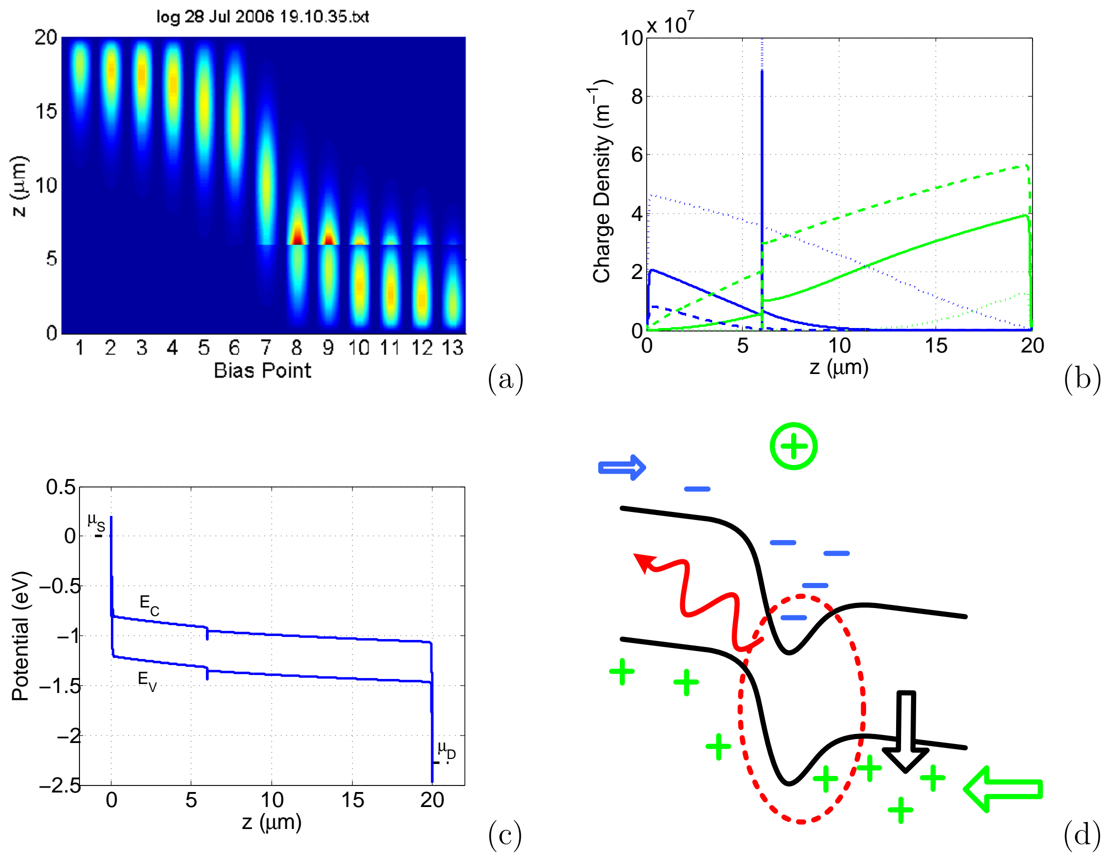

Figure 7. The presence of a charge defect (positive charge trapped in oxide at CN surface, 6μm from the source) gives rise to a fixed peak in the recombination rate (a) as the bias varies. The carrier charge profile (b) clearly shows the presence of the defect and the conditions leading to localized EL while the holes are the dominant carriers. Bias points 1 (dot), 8 (solid), and 12 (dash) are shown for electrons (left, blue) and holes (right, green). The band diagram (c) for bias point 12 highlights the effect of the defect on the band-bending, which is shown schematically in (d).

5. Conclusion

From this simulation study of EL from CNFETs using a multi-scale modeling approach, it can be concluded that the experimental observations of mobile EL, the variation in intensity of the mobile EL, fixed EL at one of the contacts, and localized EL at the site of the charge defects can all be described by attributing the EL to the direct, radiative recombination of electrons and holes. Excitonic relaxation has also been proposed as a mechanism for EL [3], but has not been incorporated in this model. The model combines a quantum mechanical approach to compute tunneling and thermionic emission currents at the contacts with a semi-classical formulation to solve long devices operating under diffusive conditions. Evaluating the effect of SB height on contact-localized EL, we conclude that a strong dependence exists, and that the EL appears when the SB height is reduced to less than 0.1eV. In all simulations, the presence of a mobile peak in EL was observed. Through an understanding of EL behaviour in CNFETs, we are better

positioned to investigate the CN-contact interface and the sensitivity of the device to charge defects through its optical properties, which may lead to novel methods for device evaluation and categorization.

Acknowledgments

The authors thank Dr. Jia Chen of the IBM T. J. Watson Research Centre for helpful technical discussions and NSERC for its financial support of this research.

[1] J. A. Misewich, R. Martel, Ph. Avouris, J. C. Tsang, S. Heinze, and J. Tersoff. Electrically induced optical emission from a carbon nanotube FET. *Science*, 300:783–786, 2003.

[2] Marcus Freitag, Vasili Perebeinos, Jia Chen, Aaron Stein, James C. Tsang, James A. Misewich, Richard Martel, and Phaedon Avouris. Hot carrier electroluminescence from a single carbon nanotube. *Nano Lett.*, 4(6):1063–1066, 2004.

[3] Marcus Freitag, James C. Tsang, , John Kirtley, Autumn Carlsen, Jia Chen, Aico Troeman, Hans Hilgenkamp, and Phaedon Avouris. Electrically excited, localized infrared emission from single carbon nanotubes. *Nano Lett.*, 6(7):1425–1433, 2006.

[4] L. Marty, E. Adam, L. Albert, R. Doyon, D. Menard, and R. Martel. Exciton formation and annihilation during 1d impact excitation of carbon nanotubes. *Phys. Rev. Lett.*, 96:136803–1–136803–4, 2006.

[5] Jia Chen, Christian Klinke, Ali Afzali, and Phaedon Avouris. Self-aligned carbon nanotube transistors with charge transfer doping. *Appl. Phys. Lett.*, 86:123108–1–123108–3, 2005.

[6] J. Tersoff, Marcus Freitag, James C. Tsang, and Phaedon Avouris. Device modeling of long-channel nanotube electro-optical emitter. *Appl. Phys. Lett.*, 86:263108–1–263108–3, 2005.

[7] Jing Guo and Muhammad A. Alam. Carrier transport and light-spot movement in carbon-nanotube infrared emitters. *Appl. Phys. Lett.*, 86:023105–1–023105–3, 2005.

[8] Jing Guo, Muhammad A. Alam, and Youngki Yoon. Theoretical investigation on photoconductivity of single intrinsic carbon nanotubes. *Appl. Phys. Lett.*, 88:133111–1–133111–3, 2006.

[9] D. L. John, Leonardo C. Castro, Jason Clifford, and David L. Pulfrey. Electrostatics of coaxial Schottky-barrier nanotube field-effect transistors. *IEEE Trans. Nanotechnol.*, 2(3):175–180, 2003.

[10] D. L. McGuire and D. L. Pulfrey. Error analysis of boundary condition approximations in the modeling of coaxially-gated carbon nanotube field-effect transistors. *Phys. Stat. Sol. (a)*, 203(6):1111–1116, 2006.

[11] Ali Javey, Jing Guo, Magnus Paulsson, Qian Wang, David Mann, Mark Lundstrom, and Hongjie Dai. High-field, quasi-ballistic transport in short carbon nanotubes. *Phys. Rev. Lett.*, 92(10):106804–1–106804–4, 2004.

[12] D. L. John, L. C. Castro, P. J. S. Pereira, and D. L. Pulfrey. A Schrödinger-Poisson solver for modeling carbon nanotube FETs. In *Tech. Proc. of the 2004 NSTI Nanotechnology Conf. and Trade Show*, volume 3, pages 65–68, Boston, U.S.A., March 2004.

[13] Mei Kei Ieong, Paul M. Solomon, S. E. Laux, Hon-Sum Philip Wong, and Dureseti Chidambarrao. Comparison of raised and schottky source/drain mosfets using a novel tunneling contact model. In *IEDM Tech. Digest*, pages 733–736, 1998.

[14] S. Selberherr. *Analysis and Simulation of Semiconductor Devices.* Springer-Verlag, New York, 1984.

[15] Jia Chen, Vasili Perebeinos, Marcus Freitag, James Tsang, Qiang Fu, Jei Liu, and Phaedon Avouris. Bright infrared emission from electrically induced excitons in carbon nanotubes. *Science*, 310:1171–1175, 2005.

[16] T. Dürkop, B. M. Kim, and M. S. Fuhrer. Properties and applications of high-mobility semiconducting nanotubes. *J. Phys.: Condens. Matter*, 16:R553–R580, 2004.

[17] G. Pennington and N. Goldsman. Semiclassical transport and phonon scattering of electrons in semiconducting carbon nanotubes. *Phys. Rev. B*, 68:045426–1–045426–11, 2003.

[18] Vasili Perebeinos, J. Tersoff, and Phaedon Avouris. Electron-phonon interaction and transport in semiconducting carbon nanotubes. *Phys. Rev. Lett.*, 94:086802–1–086802–4, 2005.

[19] Zhen Yao, Charles L. Kane, and Cees Dekker. High-field electrical transport in single-wall carbon nanotubes. *Phys. Rev. Lett.*, 84(13):2941–2944, 2000.

[20] R. Martel, T. Schmidt, H. R. Shea, T. Hertel, and Ph. Avouris. Single- and multi-wall carbon nanotube field-effect transistors. *Appl. Phys. Lett.*, 73(17):2447–2449, 1998.

[21] S. Heinze, J. Tersoff, R. Martel, V. Derycke, J. Appenzeller, and Ph. Avouris. Carbon nanotubes

as Schottky barrier transistors. *Phys. Rev. Lett.*, 89(10):106801–1–106801–4, 2002.

[22] J. Appenzeller, J. Knoch, V. Derycke, R. Martel, S. Wind, and Ph. Avouris. Field-modulated carrier transport in carbon nanotube transistors. *Phys. Rev. Lett.*, 89(12):126801–1–126801–4, 2002.

[23] Zhihong Chen, Joerg Appenzeller, Joachim Knoch, Yu-Ming Lin, and Phaedon Avouris. The role of metal-nanotube contact in the performance of carbon nanotube field-effect transistors. *Nano Lett.*, 5(7):1497–1502, 2005.

[24] R. Martel, V. Derycke, C. Lavoie, J. Appenzeller, K. K. Chan, J. Tersoff, and Ph. Avouris. Ambipolar electrical transport in semiconducting single-wall carbon nanotubes. *Phys. Rev. Lett.*, 87(25):256805–1–256805–4, 2001.